

EFFECTS OF UNDERGROUND TOPOGRAPHICAL IRREGULARITY TO SEISMIC AMPLIFICATION IN THE NOBI PLAIN

K TANAKA¹, O KURIMOTO² And N FUKUWA³

SUMMARY

The underground structure of the Nobi plain has step-like topographic irregularity along the Yoro faults in the west of the plain. Therefore, strong earthquakes can cause "the damage belt" in the Nobi plain, as in Kobe during the 1995 Hyogo-ken Nanbu earthquake. In order to estimate the influence of the irregularity on seismic amplification, two- and three-dimensional wave propagation analyses were performed. The results indicated that the irregularity of deep ground structure near the Yoro faults causes large amplification locally in the Nobi plain, and that the location of the zones of large amplification varies with the predominant frequency of incident wave, predominant direction of seismic motion, and the bedrock shape at the basin edge.

INTRODUCTION

The 1995 Hyogo-ken Nanbu earthquake caused extreme damage in and around Kobe city, and the heavily damaged zone, which was called "damage belt", occurred. It was indicated that the deep basin edge structure along the Rokko faults in the Kobe area mainly affected the amplification of seismic ground motions. In the west part of the Nobi plain, the underground basin edge structure has step-like topographical irregularity along the Yoro fault. It is expected that an earthquake will cause the damage belt zone in the Nobi plain analogous to Kobe case, because of similarity of the basin edge structures.

In this paper, we performed wave propagation analyses on the Nobi plain considering the deep underground irregular structure, and examined effects of the irregularity to seismic amplification in the plain. The sedimentary basin structure was modeled in east-west section normal to the Yoro fault. Seismic responses on the surface of the model were evaluated using two-dimensional(2-D) elastic wave propagation analyses. Differences between out-of-plane(SH wave) motion and in-plane(SV wave) motion, and effects of the predominant frequency of incident wave were discussed. Moreover, seismic responses by three-dimensional(3-D) wave propagation analysis were evaluated and compared to the results of 2-D case.

DEEP BASIN STRUCTURE MODEL OF THE NOBI PLAIN

The Nobi plain consists of a sedimentary basin structure; layers and bedrock of the basin are gradually dipping to the west. The area of the plain is approximately 30km wide in east-west(EW), 40km long in north-south(NS). Bedrock is outcropped in the east of the plain, while the thickness of the sediments overlying bedrock is about 2-3km in the west. The underground structure changes abruptly at the western edge of the sedimentary basin, and basement layer forms step-like structure along the Yoro fault.

In the Nobi plain, refraction surveys[e.g., Masaki et al., 1982a] and reflection surveys[e.g., Sugai et al., 1998] have been conducted. Several 2-D subsurface structures were proposed for survey-lines. Masaki et al. (1982b) proposed a 2-D subsurface structure model in the east-west cross-section across the central part of the plain, by compiling underground structure information from refraction surveys and surface geology. The section line of the model is represented in Figure 1.

¹ Technical Research Institute, Obayashi Corporation, Tokyo, Japan Email: tanakak@tri.obayashi.co.jp

² Technical Research Institute, Obayashi Corporation, Tokyo, Japan

³ CCRAST, Nagoya University, Nagoya, Japan Email: fukuwa@sharaku.nuac.nagoya-u.ac.jp

Based on the 2-D model proposed by Masaki et al. (1982b), the basin structure for analysis was constructed. In the model by Masaki et al., the structure near the Yoro fault is not clear, and its basement shape at the western basin edge is modeled as about 40° dip. However, the basement shape at the western basin edge near the Yoro faults is considered as steep reverse dip shape. Therefore, the edge shape was modified to be vertical, 90° dip in the analysis model(Model-A in Figure 2). Additionally two structure models with different edge shape were constructed; one of the edge shape is 60° dip(Model-B in Figure 2) and the other is 40° dip(Model-C in Figure 2). The sediments consist of three layers whose shear wave velocities are 400, 680, and 1600m/s, respectively. The velocity and density profiles in each layer are listed in Table 1. The damping Q values(quality factors) are determined from shear wave velocity Vs as $Q=Vs[m/s]/10$.



Figure 1: Location of the East-west Cross-section Model.

Table 1: Velocity Model of the Sedimentary Basin.

	Vp (km/s)	Vs (km/s)	Density (tf/m ³)	Q
Sediment-1	1.8	0.4	2.0	40
Sediment-2	2.0	0.68	2.1	68
Sediment-3	3.0	1.6	2.3	160
Basement	5.0	2.8	2.6	280

Table 2: Fault Parameters of the Hypothetical Yoro Fault.

Strike	Dip	Rake	Length	Width	Seismic Moment
N333°E	90°	90°	30km	20km	2.96E+26 dyne*cm
Magnitude	Rise Time	Rupture Type	S wave	Rupture	
6.8	3.0 sec	radial	3.3 km/s	2.5 km/s	

SEISMIC RESPONSE ANALYSIS USING 2-D MODEL

Effects of the Irregular Structure to Seismic Amplification

Seismic response on the surface of the 2-D model was evaluated by out-of-plane(SH wave) response analyses using 2-D finite difference(FD) method[Kaneda et al., 1996]. The FD model of the EW section is 48.4km wide and 3.4km deep. The grid spacing is set at 8m, which gives a frequency resolution limit of 5Hz within the lowest velocity($Vs=400m/s$) regions of the model. The excitation was an incident plane SH wave propagating vertically upwards and incoming uniformly at bottom of the model. Two pulse waveforms shown in Figure 3 were used as the input waves; one has the short duration time $T=0.6sec$, and the other has the long duration time $T=8sec$ (hereafter: called short pulse wave, and long pulse wave, respectively). The short pulse wave is effective in the frequency range 0-5Hz. The duration time of the long pulse wave is corresponding to the predominant period of 1st mode of transfer function relating ground motions to the incident wave at the west of the plain. Synthetic bedrock motions of the hypothetical Yoro fault earthquake[Tanaka et al., 1998], which were obtained at the center of the model (site-A in Figure 1) by using the stochastic synthesis method[Kamae et al., 1991], were also used as seismic incident waves. Table 2 shows fault parameters of the hypothetical Yoro fault earthquake, and Figure 3(c) shows the synthetic waveforms.

Distributions of maximum values on the surface of the model are shown in Figure 4. In cases of the short pulse wave incidence and the synthetic Yoro earthquake, the distribution of maximum response shows large amplification peaks near at eastern and western basin edge. The distribution for the long pulse wave incidence has large peaks near at western basin edge. Remarkable is the peak at western edge with vertical bedrock structure of the Yoro fault; amplification of the peak is very large, and its width is narrow. In the region from the central part to the west part of the basin, the maximum responses have gentle peaks at the points $X=30-35km$ and $X=40-46km$.

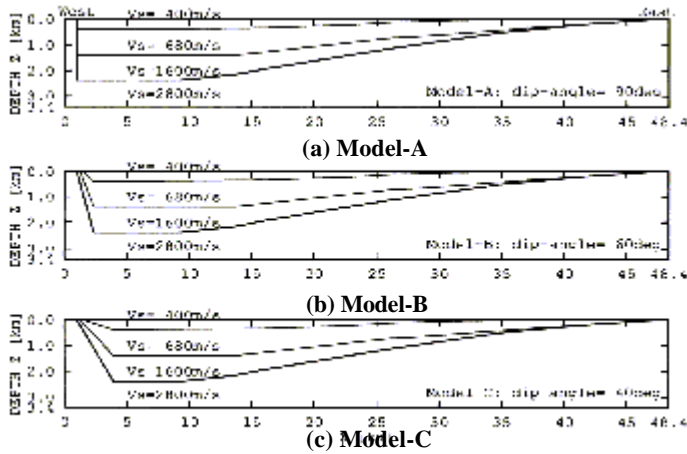
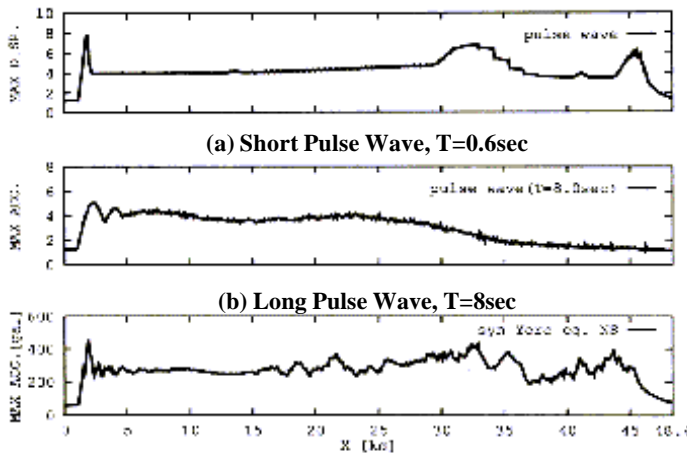


Figure 2: 2-D Structure Models for analysis.



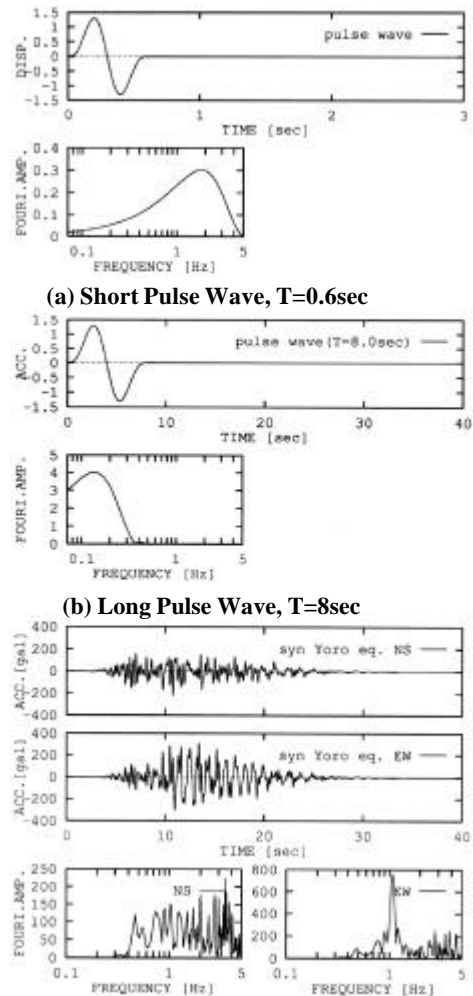
(c) Synthetic Yoro Earthquake

Figure 4: Maximum Response on the surface of

Figure 5 compares the transfer functions relating ground motions to the incident wave at 16 sites on the surface, between the one-dimensional(1-D) elastic model using the soil column at each sites(Figure 5(a)) and the 2-D model including the irregular structure(Figure 5(b)). In the region from the middle west part of the plain to the east (at $X=4.0-48.4\text{km}$), the transfer functions have small differences between the 2-D and the 1-D cases(Figure 6(a)), that is, amplification is mainly affected by 1-D site effect. The 2-D transfer function at the point $X=1.8\text{km}$ (Figure 6(b)) has larger amplitude than the 1-D case in the frequency range 1.8-4Hz. This result indicates that amplification at the western basin edge includes the effects related to the 2-D irregular structure, that is, 2-D site effect.

The time-histories of the surface response for the short pulse wave incidence, are shown in Figure 7. The amplification peak at the western edge of the basin is locally created by constructive interference between the basin edge diffracted waves and the direct S waves, as pointed out in Kobe case[e.g., Kawase, 1996]. The basin diffracted waves propagate inside the basin, while the direct S waves propagate upward from the underlying bedrock. In the zone where these two waves coincide, the amplitude of the ground motions is strongly amplified by interference.

The time-histories also indicate that three waves propagate on the surface with the different velocities; the velocities for Wave-A, B and C are approximately 400m/s, 700m/s, and 2000m/s, respectively. Figure 8 shows dispersion curves of surface waves for the 1-D structure near western basin edge ($X=1.0-9.2\text{km}$). Predominant frequencies of the three waves are about 1-2Hz. In this frequency range, phase velocities of Love waves are 400m/s for fundamental mode, and approximately 700m/s for 2nd and 3rd modes.



(c) Synthetic Yoro Earthquake

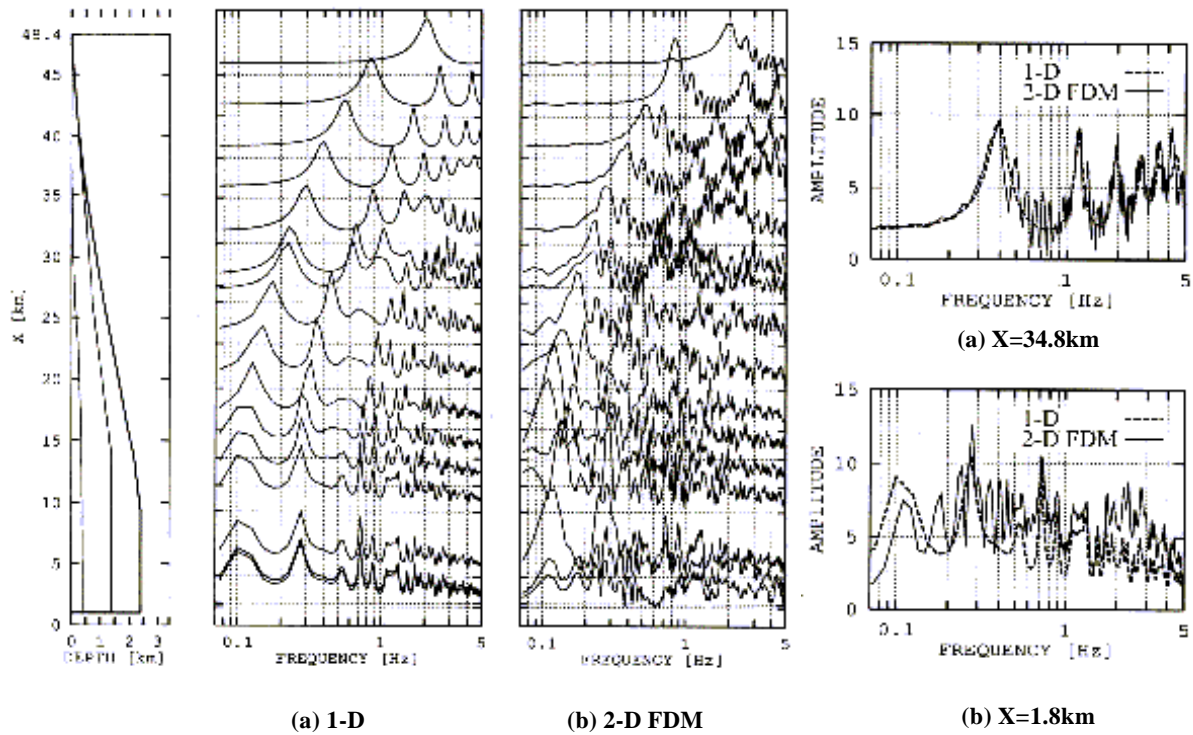


Figure 5: Transfer Functions.

Figure 6: Comparison of Transfer Functions.

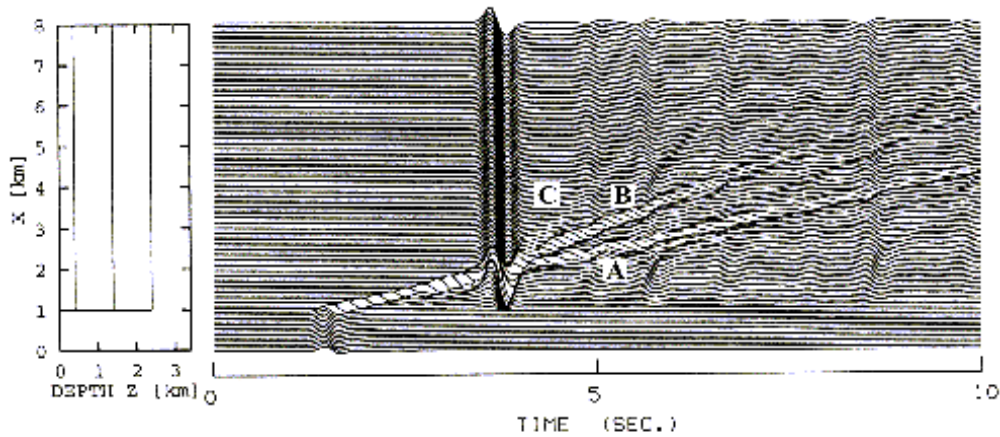


Figure 7: Response Time Histories to the Short Pulse Wave Incidence (SH motion).

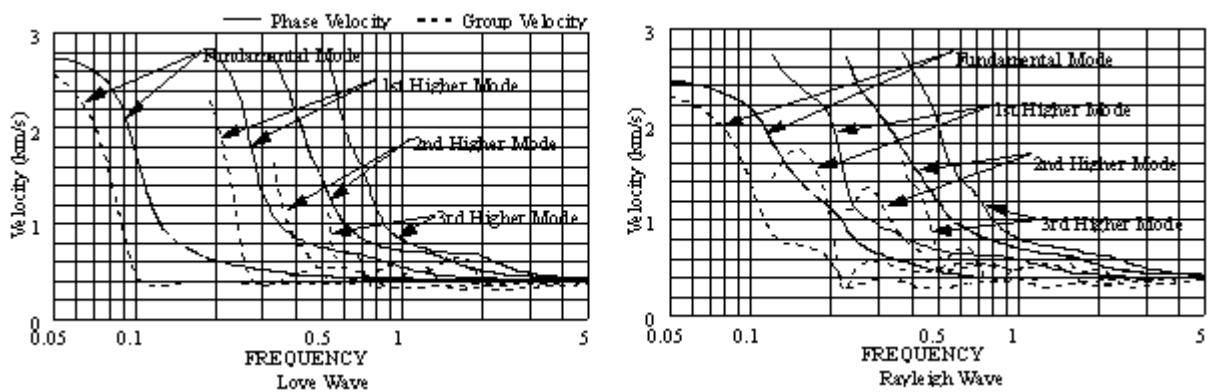


Figure 8: Theoretical Dispersion Curves of Surface waves for the 1-D Soil Structure at the West of the Nobi Basin, i.e., $X=1.0-9.2\text{ km}$ in Model-A.

Comparison of SH and SV Motion at Basin Edge

With the model of the basin edge underground structure near the Yoro fault, seismic response analyses of out-of-plane(SH) and in-plane(SV) motion were carried out by using 2-D finite element method(FEM). The model

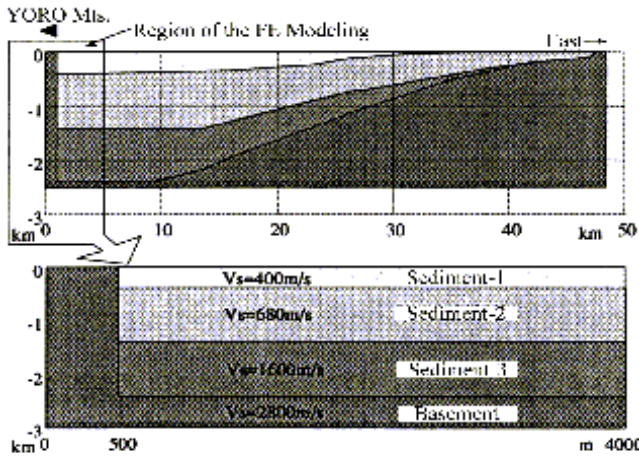


Figure 9: Region of the Basin Structure for 2-D FEM analysis.

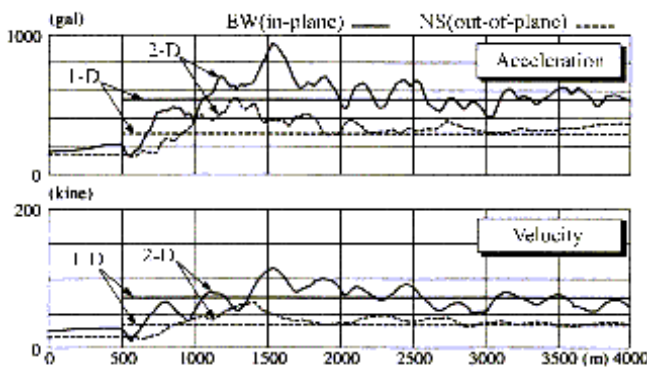


Figure 10: Maximum Response to the Incidence of the Synthetic Yoro Earthquake.

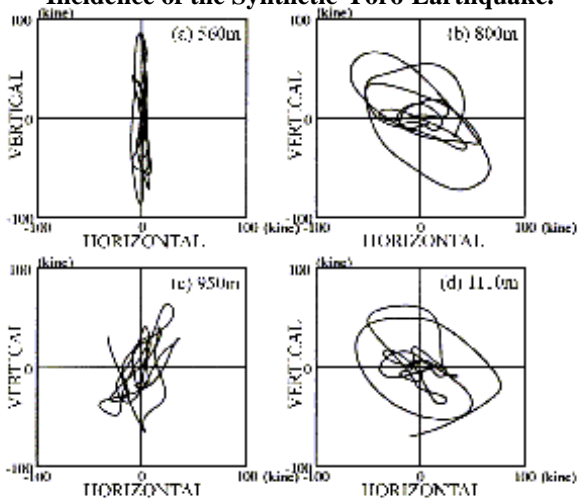


Figure 11: Vertical Particle Motions at the Points of Local Maximum & Minimum of Horizontal Response.

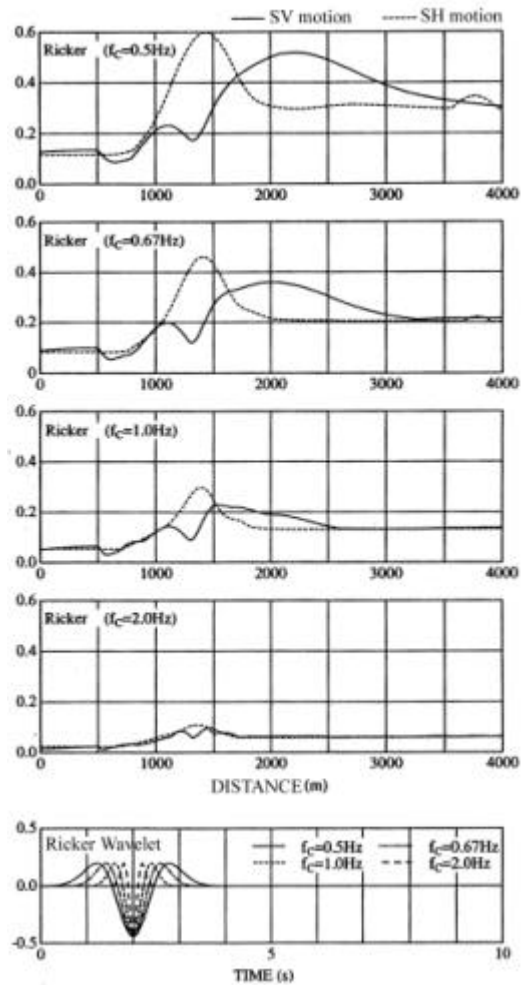


Figure 12: Maximum Response to the Ricker Wavelets.

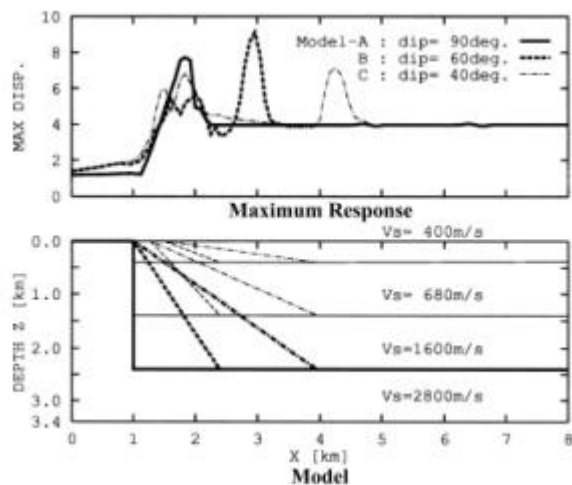


Figure 13: Comparison of the Maximum Response Distributions to the Pulse Incidence between the Three Models.

and its range is represented in Figure 9. The FE mesh is generated to give a frequency resolution limit of 5Hz. Response analyses were performed in frequency domain, for vertical incidence of SH and SV waves.

The distributions of maximum response to the incident waves of the synthetic Yoro earthquake are shown in Figure 10. The peak positions of maximum responses vary with cases of in-plane or out-of-plane wave. The out-of-plane response(NS component) have a maximum amplification peak closer to the basin edge than the horizontal in-plane response(EW component). Some periodic peaks of local maximum and local minimum are seen in the maximum velocity distribution of in-plane response. These peaks of local maximum and local minimum in the horizontal velocity response appear in the orbit motions presented in Figure 11.

Figure 12 shows the distributions of maximum response to the incidence of the Ricker wavelet with four cases of central frequency, i.e., $F_c=0.5\text{Hz}$, 0.67Hz , 1.0Hz , and 2.0Hz . The peaks in out-of-plane response are closer to the basin edge than in in-plane response, same as the case of the synthetic seismic motion. The peak distribution of in-plane responses is influenced by predominant frequency of incident wave. The peak positions of the in-plane responses vary with the central frequency of incident Ricker wavelet, while the peak positions of the out-of-plane responses vary slightly. In the theoretical dispersion curves(Figure 8), phase and group velocities of Rayleigh waves are larger than those of Love waves. This characteristic of surface waves may cause differences between in-plane responses and out-of-plane responses.

Effects of Basin Edge Shape to Seismic Response

The seismic amplification in the west of the Nobi plain is affected by the basin edge structure near the Yoro fault. However, the deep subsurface structure of the Nobi basin is not explored in detail, and the basement shape at the basin edge is not clearly investigated. Therefore, the influence of the basement shape was examined using the model with different basin edge structures.

Ground motions were computed using the 2-D FD models whose western edge shapes are dipping 60° (Model-B in Figure 2) and 40° (Model-C in Figure 2). The distributions of the maximum response to the short pulse SH incidence are shown in Figure 13.

At the western basin edge, the seismic response varies according to the bedrock shape. In the case of 60° and 40° dip, another large peak appears inside the basin, and seems to be created by focusing effect between the direct S waves from dipping layer and horizontal layer. The peak, which is created by interference between the basin edge diffracted waves and the direct S waves, also appears close to the basin edge. This result indicates that it is important for estimation of seismic amplification to clarify and identify the underground structure of basin edge in detail.

SEISMIC RESPONSE ANALYSIS USING 3-D MODEL

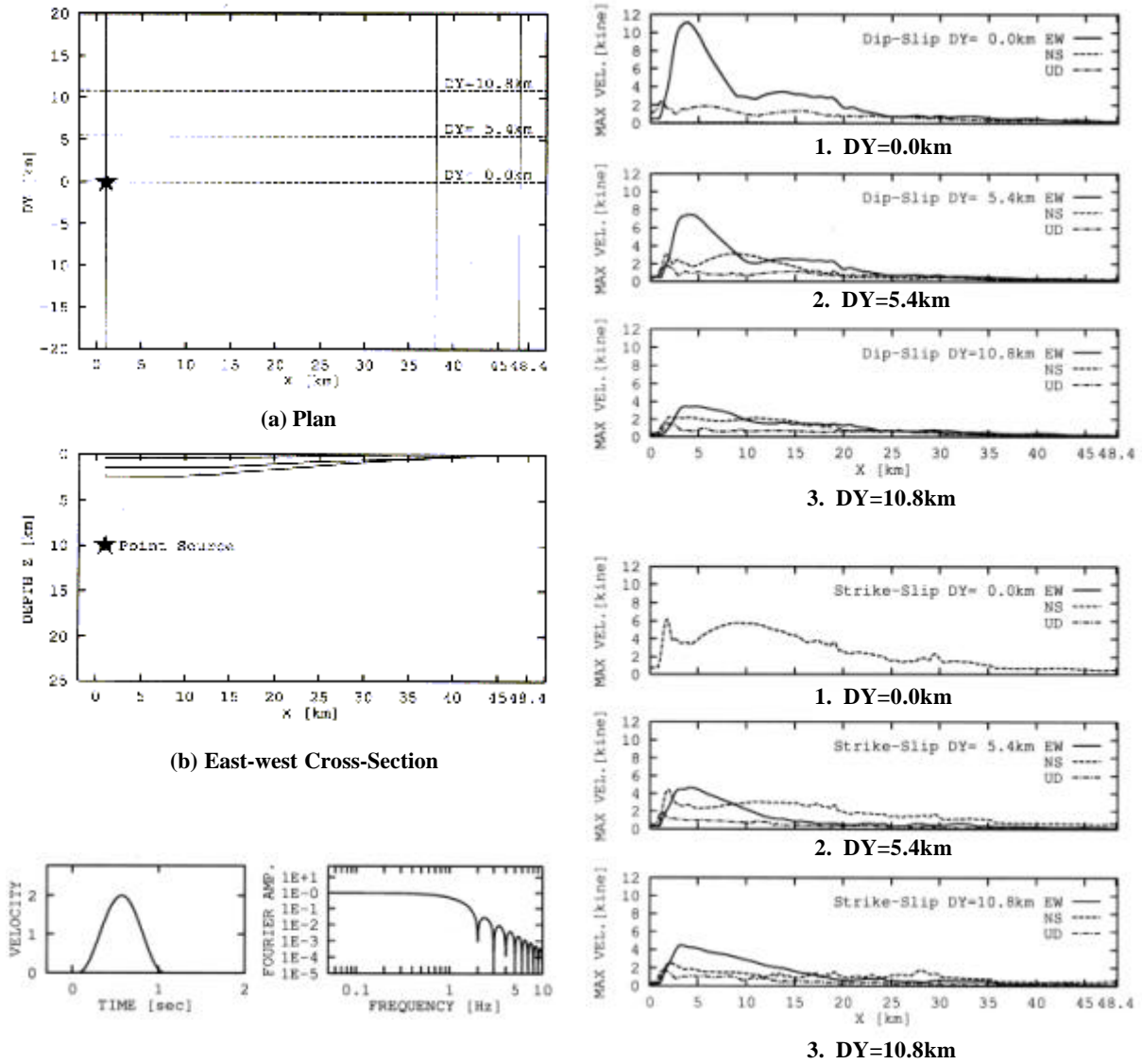
Seismic responses on the surface of the basin to a point source were evaluated by 3-D wave propagation analysis using 3-D finite difference method[Pitarka et al., 1996]. The 3-D elastic model, which have 2-D basin structure, was constructed by extending the 2-D model of the east-west(EW) section(Model-A) to north-south(NS) direction. The model is shown in Figure 14. It is 39.96km long, 52.2km wide, and extends to a depth of 25.02km. A grid spacing of 0.18km is used, which gives a frequency resolution limit of 0.444Hz ($T > 2.25\text{sec}$ in period) within the lowest velocity($V_s=400\text{m/s}$) regions of the model. The damping Q values[Graves, 1996] are set at a reference frequency 0.2Hz ($T_q=5.0\text{sec}$ in period).

A vertical dip-slip source and a horizontal strike-slip source were used as a point source, which was located at 10.08km in depth under the basin edge interface. A cosine-shaped slip rate function was used. The rise time is set at 1sec. Figure 15 shows the slip rate function. Fault parameters for the point sources are listed in Table 3.

Figure 16 shows the distributions of the maximum responses on the surface, which are in the lines 0km, 5.4km and 10.8km apart from the epicenter. As shown by the results of the 2-D analyses with out-of-plane and in-plane motion, the peak positions vary with the direction of components of the ground motion in 3-D wave propagation analysis. The peaks of the NS component, which is corresponding to 2-D out-of-plane motion, are located closer to the basin edge than those of the EW component, which is corresponding to in-plane motion. This result seems to reflect differences of characteristics of two surface waves, Love and Rayleigh wave.

Table 3: Fault Parameters of Point Sources used in 3-D analysis.

Event	Strike	Dip	Rake	Depth	Seismic Moment	Rise Time
Dip-slip	N180°E	90°	90°	10.08km	1.0E+24 dyne*cm	1.0 sec
Strike-slip	N180°E	90°	0°			



CONCLUSIONS

1. In the region from the middle west to the east of the Nobi plain, where the sedimentary layers are gradually dipping, seismic amplification is mainly affected by 1-D site effect. In the region near the Yoro fault in the west of the plain, seismic amplification is affected by 2-D site effect of the irregular basin edge structure; the irregularity of deep ground structure near the Yoro fault may cause local large amplification of seismic motion.
2. The distribution and its peak position of the maximum ground responses, which are amplified by 2-D site effect of irregular structure, are different for the incidence of out-of-plane motion and in-plane motion. The in-plane motion of seismic response is influenced by the predominant frequency of incident wave.
3. The distribution of maximum seismic response varies according to the bedrock shape at the basin edge near the Yoro fault. It is, therefore, necessary to clarify and identify the deep underground structure of the basin edge in detail.

ACKNOWLEDGEMENTS

The 2-D FDM code used for wave propagation analyses was made by Dr. T. Seki of Technical Research Institute, Obayashi Corporation. The authors would like to express their gratitude to Prof. K. Irikura and Dr. T. Iwata of Disaster Prevention Research Institute, Kyoto University for suggestions about 3-D FDM.

REFERENCES

1. Graves, R. W. (1996), "Simulating seismic wave propagation in 3D elastic media using staggered-grid finite differences", *Bull. Seism. Soc. Am.*, Vol.86, No.4, pp.1091-1106
2. The Japanese Geotechnical Society, Chubu branch (1988), *Geotechnical data of subsoils in Nagoya.*, (in Japanese)
3. Kamae, K., Irikura, K. and Fukuchi, Y. (1991), "Prediction of strong ground motion based on scaling law of earthquake - By stochastic synthesis method", *J. Struct. Constr. Eng., AIJ*, No.430, pp.1-9, (in Japanese)
4. Kawase, H. (1996), "The cause of the damage belt in Kobe: "the basin-edge effect," constructive interference of the direct S-wave with the basin-induced diffracted/Rayleigh waves", *Seism. Res. Lett.*, 67, No.5, pp.25-34
5. Kaneda, Y., Seki, T. and Ejiri, J. (1996), "Seismic simulation on stochastic synthesis method and finite difference method for the prevention of earthquake disaster", *Butsuri-tansa*, Vol.49, No.6, pp.562-573, (in Japanese)
6. Masaki, K., Taniguchi, H. and Iida, K. (1982a), "On the ground structure of Nagoya area. II - Observations of seismic waves generated from the 2nd Nagoya-Nabeta and the 1st Toyohashi-Tahara explosions", *Bulletin of Aichi Institute of Technology*, No.17B, pp.159-171, (in Japanese)
7. Masaki, K., Taniguchi, H. and Iida, K. (1982b), "Predominant period and mean amplitude of long period microtremor measured in the Nobi plain and their relations to ground structure", *Butsuri-tanko (Geophysical Exploration)*, Vol.35, No.1, pp.1-12, (in Japanese)
8. Miyazaki, T. et al. (1985), "Synthetic research of microseisms in the Nohbi plain - Comparison of observational results with vibrational analysis", *J. Struct. Constr. Eng., AIJ*, No.351, pp.103-112, (in Japanese)
9. Pitarka, A. and Irikura, K. (1996), "Modeling 3D surface topography by finite-difference method : Kobe-JMA station site, Japan, case study", *Geography. Res. Lett.*, Vol.23, No.2, pp.2729-2732
10. Sugai, T. and Sugiyama, Y. (1998), "Deep seismic reflection survey of concealed active structures in the Nobi Plain, central Japan", *Geological Survey of Japan, Interim Report, Interim Report on Active Fault and Paleoeearthquake Researches in the 1997 Fiscal Year*, no.EQ/98/1, p.55-65, (in Japanese)
11. Toda, S. et al. (1997), "Subsurface structure and activities of the Yoro fault - seismic reflection survey in Tado town, Mie prefecture, central Japan-", *Zisin (J. Seism. Soc. Jap)*, second series, Vol.49, pp.429-440, (in Japanese)